RSC Sustainability

ROYAL SOCIETY OF CHEMISTRY

PAPER

View Article Online
View Journal | View Issue

Cite this: *RSC Sustainability*, 2025, **3**, 3964

Thermoelectrically powered CO_2 conversion in a reactive carbon electrolyzer†

Abhishek Soni, ‡[a] Siwei Ma,‡[a] Giuseppe V. Crescenzo[a] and Curtis P. Berlinguette *[abcd]

Received 28th December 2024
Accepted 9th May 2025

DOI: 10.1039/d4su00826j

rsc.li/rscsus

Here, we use thermoelectric generators to power reactive carbon electrolyzers that upgrade captured CO_2 into fuels and valuable chemicals. Reactive carbon electrolyzers convert the liquid eluent from a direct air capture unit—referred to as the "reactive carbon solution". Thermoelectric generators convert temperature differences into electrical energy, enabling the use of waste heat to power the reactive carbon electrolyzers. This configuration enables operation without reliance on solar and wind power. We report the experimental demonstration of a thermoelectric generator powering a reactive carbon electrolyzer.

Sustainability spotlight

Rising levels of atmospheric CO_2 demands innovative and sustainable solutions for carbon capture and conversion. This study integrates thermoelectric generators with reactive carbon electrolyzers to transform captured CO_2 into fuels and valuable chemicals. Thermoelectric generators sustainably power reactive carbon electrolyzers by utilizing waste heat, thereby reducing reliance on traditional energy sources. The use of liquid reactive carbon feedstocks (*e.g.*, bicarbonate) instead of gaseous CO_2 enhances system efficiency and impurity tolerance, addressing common limitations of gaseous CO_2 electrolysis. We demonstrated the feasibility of our technology under conditions relevant to low-temperature geothermal plants and potential Mars colonization. This work highlights the importance of several UN Sustainable Development Goals: affordable and clean energy (SDG 7), industry, innovation, and infrastructure (SDG 9), and climate action (SDG 13).

Introduction

Carbon capture and utilization technologies are being implemented to mitigate rising atmospheric CO_2 levels.[1–7] Among these technologies, reactive carbon electrolyzers offer a promising approach for electrochemically converting CO_2 into fuels and chemicals using liquid (bi)carbonate feedstocks derived from direct air capture.[1,8–14] However, their widespread deployment is often limited by their dependence on clean electricity.[15]

To address this limitation, waste heat from industrial processes or natural thermal gradients can be harnessed by thermoelectric materials as a sustainable power source for reactive carbon electrolyzers. Thermoelectric materials convert temperature differences directly into electrical energy (*i.e.* voltage, *V*):[16]

$$V = S\Delta T \quad (1)$$

where *S* is the Seebeck coefficient.[17] Thermoelectric materials are widely used in aerospace,[18,19] solar-thermal systems,[20,21] and remote power generation[22,23] due to the lack of moving parts,[24] low cost,[25] and durability.[26] By integrating thermoelectric generators with reactive carbon electrolyzers, we present a proof-of-concept for a sustainable, resilient, and easily deployable CO_2 conversion system using commercially available catalysts.

Experimental

Materials

Silver and copper nanoparticles (25–45 nm, 99.5% trace metals basis), were purchased from Sigma-Aldrich. Potassium hydroxide (KOH) and potassium bicarbonate $KHCO_3$ (99.9%) were purchased from Alfa Aesar. Nickel foam (>99.99%) was purchased from MTI Co. Fumsep FBM bipolar membranes (BPMs) were purchased from Dioxide Materials (USA) and soaked in 1 M NaCl for 24 h prior to use. Pure 99.999%, CO_2 (99%), and Ar (99.999%) gasses were purchased from Praxair Canada Inc. The carbon paper (H23 Freudenberg, Nafion™

[a]*Department of Chemistry, The University of British Columbia, 2036 Main Mall, Vancouver, British Columbia, V6T 1Z1, Canada. E-mail: cberling@chem.ubc.ca*

[b]*Department of Chemical and Biological Engineering, The University of British Columbia, 2360 East Mall, Vancouver, British Columbia, V6T 1Z3, Canada*

[c]*Stewart Blusson Quantum Matter Institute, The University of British Columbia, 2355 East Mall, Vancouver, British Columbia, V6T 1Z4, Canada*

[d]*Canadian Institute for Advanced Research (CIFAR), 661 University Avenue, Toronto, Ontario, M5G 1M1, Canada*

† Electronic supplementary information (ESI) available. See DOI: https://doi.org/10.1039/d4su00826j

‡ Contributed equally.

Dispersion; D-520 dispersion, 5% w/w in water and 1-propanol) was purchased from Fuel Cell Store (USA). Commercial thermoelectric generators were obtained directly from Amazon and custom thermoelectrics. Unless otherwise noted, all materials were used as received.

A CH Instruments 660D potentiostat (USA) equipped with an Amp booster was used for all electrolysis experiments driven by potentiostat. A gas chromatograph (PerkinElmer, Clarus 580) equipped with a packed MolSieve 5 Å column and a HayeSepD column was used to detect CO and H_2 using a flame ionization detector and a thermal conductivity detector, respectively. The carrier gas was N_2 (99.999%, Praxair Canada Inc.). The concentrations of the products CO, and H_2 (ppm) in the headspace of the catholyte reservoir were quantified using previously constructed calibration curves for CO and H_2.

Catalyst and electrolyzer preparation

For reactive carbon electrolyzer experiments, the cathodes were fabricated by automated spray coating of silver nanoparticles onto an H23 Freudenberg carbon paper at a mass loading of 1.8 mg cm^{-2}. The spray-coater was built from an ultrasonic nozzle (Microspray, USA) mounted to a custom motorized XYZ gantry system (Zaber Technologies Inc., Canada) above a hotplate (PC-420D, Corning, USA). To prepare the stock solution of the silver-containing catalyst ink, 400 mg of the metal nanoparticles were suspended in 20 mL of isopropyl alcohol with 60 μL of Nafion (D-520 dispersion, 5% w/w in water and 1-propanol).

The catalyst materials were then integrated into a membrane electrode assembly (MEA; 2 cm × 2 cm) along with a nickel foam anode (MTI Co.) and a BPM (FumaSEP). The MEA was sandwiched between a custom-made, in-house built titanium cathode flow plate and a stainless steel anode flow plate (size: 6 cm × 6 cm × 1.2 cm). Two stainless steel housing plates fastened with eight M6 bolts compressed the MEA and flow plates. For the scaled-up electrolyzer, the materials and flow plate design remained the same as those of the 4 cm^2 electrolyzer, except that the MEA dimensions were increased to 100 cm^2.

For the thermoelectrically-driven reactive carbon electrolyzer experiments, one peristaltic pump delivered a 1 M KOH solution to the anode compartment at a flow rate of 30 mL min^{-1}, and another delivered a 3 M $KHCO_3$ solution at a flow rate of 100 mL min^{-1} to the cathode. A flow rate of 160 sccm of N_2 was supplied to the headspace of the catholyte reservoir, acting as a carrier gas towards the gas chromatograph. The products from the cathodic reaction (CO, CO_2, and H_2) were passed into an in-line gas chromatograph (SRI-8610C) for analysis (ESI Fig. S1†).

Thermoelectric generators

We tested various commercially available thermoelectric generators for open circuit voltage and output current at ΔT = 100 °C.[27] The commercially available "TEG-287-1.4-1.5" produced the highest open circuit voltage (1.22–1.25 V) and current (185–200 mA) (ESI Fig. S2†). We used three of these thermoelectric generators in series (hereafter referred to as "TEG") for all reactive carbon electrolyzer experiments. A Kamtop digital K-type digital thermocouple (Amazon) was used to measure the temperature at the hot (T_{hot}) and cold (T_{cold}) faces of the TEG. The TEGs generate an open circuit voltage of ~3.6 V and an output current of 200 mA at ΔT = 100 °C (T_{hot} = 25 °C and T_{cold} = −75 °C). The T_{cold} was accessed by using a cryogenic ice bath of dry ice and ethanol.[28] We confirmed that the open circuit voltage was maintained over 12 hours.

Thermoelectric reactive carbon electrolysis

The heat-driven reactive carbon electrolysis experiments were performed by connecting the TEG to the reactive carbon

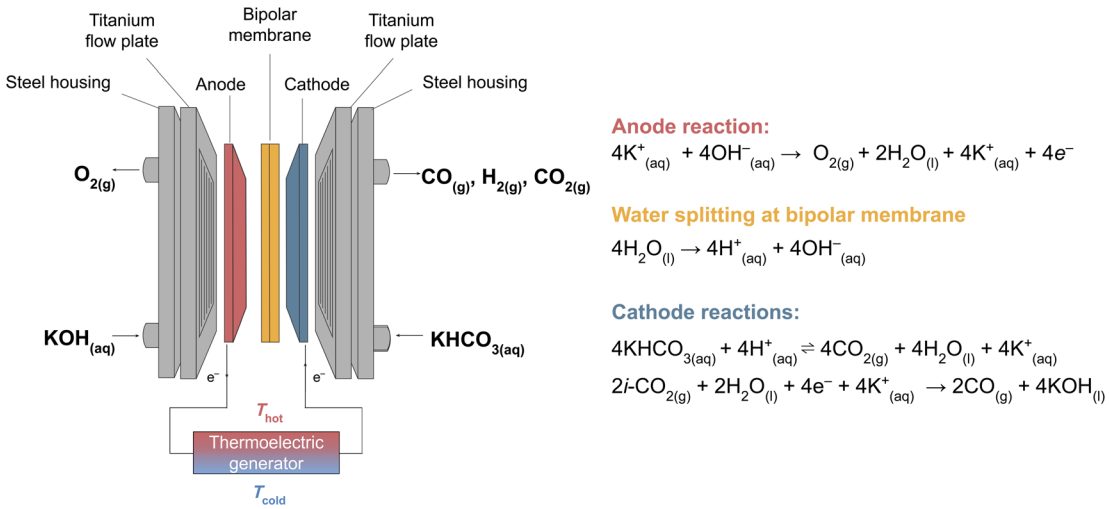

Fig. 1 A thermoelectrically-powered reactive carbon electrolyzer. Schematic of an exploded view of the zero-gap reactive carbon electrolyzer connected to the thermoelectric generator (not drawn to scale) used in this study and the accompanying electrochemical reactions at each component of the electrolyzer.

electrolyzer (ESI Fig. S3†). The positive terminal of the TEG was connected to the anode and the negative terminal was connected to the cathode (Fig. 1 and ESI Fig. S3†). A multimeter was embedded into the circuit to monitor the real-time voltage and current across the reactive carbon electrolyzer. The gaseous species emerging from the cathode outlet were passed to an in-line gas chromatograph for analysis.

Faradaic efficiency

We measured the CO and H_2 selectivity at a constant current density by quantifying their respective concentrations as a mole fraction, χ_k, where k = CO or H_2 by gas chromatography. The selectivity is often used interchangeably with the Faradaic efficiency of gaseous product k (FE_k, eqn (2)):[9]

$$FE_k = \frac{n_k F \chi_k F_m}{I} \quad (2)$$

where n_k is the number of electrons exchanged, F is Faraday's constant ($F = 96\,485$ C mol^{-1}), F_m is the molar flow rate in mol s^{-1}, and I is the total current in A produced from the TEG or the potentiostat. The molar flow rate is derived from the volume flow rate F_m by the relation $F_m = pF_v/RT$, with p being the atmospheric pressure in Pa, R the ideal gas constant of 8.314 J mol^{-1} K^{-1} and T is the temperature in K.

Results and discussion

Thermoelectrically-driven reactive carbon electrolysis

The reactive carbon electrolyzers used in this study introduce an aqueous potassium bicarbonate ($KHCO_3$) feedstock solution into the cathode compartment (Fig. 1). Reactive carbon electrolyzers utilize liquid (bi)carbonate to deliver high concentrations of captured CO_2 to the cathode, facilitating efficient electrochemical reactions with improved CO_2 utilization efficiencies[29] and reduced sensitivity to impurities.[30,31]

In the electrolyzer, bicarbonate reacts with protons (H^+) generated by water dissociation at the bipolar membrane (BPM), as described in eqn (3), to produce CO_2 *in situ* (*i*-CO_2; eqn (4)). This *i*-CO_2 is subsequently reduced at the cathode to form carbon monoxide (CO), according to eqn (5). At the anode, the electrolyzer is supplied with an aqueous KOH solution to support the oxygen evolution reaction (OER), producing oxygen gas (O_2) as shown in eqn (6). Meanwhile, hydroxide ions (OH^-) generated at the BPM interface are transported through the BPM to the nickel anode.

$$\text{Water dissociation: } 4H_2O_{(l)} \rightarrow 4H^+_{(aq)} + 4OH^-_{(aq)},\ E^o = 0.8\ V \quad (3)$$

$$\text{}i\text{-}CO_2\text{ generation: } 4KHCO_{3(aq)} + 4H^+_{(aq)} \rightleftharpoons 4i\text{-}CO_{2(g)} + 4H_2O_{(l)} + 4K^+_{(aq)} \quad (4)$$

$$\text{}i\text{-}CO_2\text{ reduction: } 2i\text{-}CO_{2(g)} + 2H_2O_{(l)} + 4e^- + 4K^+_{(aq)} \rightarrow 2CO_{(g)} + 4KOH_{(aq)},\ E^o = -0.11\ V \quad (5)$$

$$\text{OER: } 4K^+_{(aq)} + 4OH^-_{(aq)} \rightarrow O_{2(g)} + 2H_2O_{(l)} + 4K^+_{(aq)} + 4e^-,\ E^o = 1.23\ V \quad (6)$$

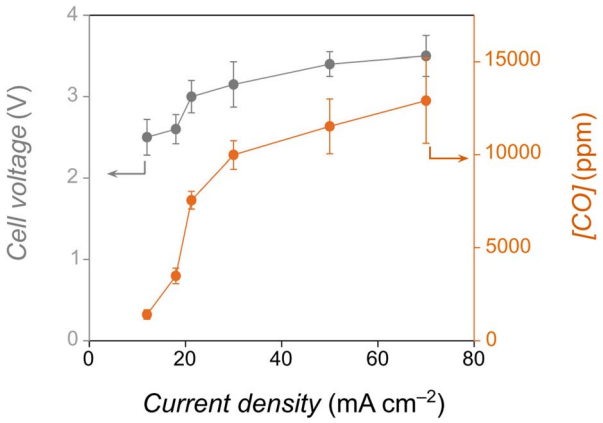

Fig. 2 Benchmark reactive carbon electrolysis experiments that measured the amount of CO produced as a function of applied current by a potentiostat. The error bars represent the standard error from n = 3 independent experiments.

As an initial benchmark, we performed reactive carbon electrolysis experiments using a potentiostat equipped with an amp booster. For each experiment, the cathode was supplied with a 3 M $KHCO_3$ aqueous solution at a flow rate of 100 mL min^{-1}, while the anode was supplied with 1 M KOH at 30 mL min^{-1} that was continuously recirculated. We observed that the cell voltage increased from 2.5 V to 3.5 V as the current density increased from 12 mA cm^{-2} to 70 mA cm^{-2} (Fig. 2; shown in gray). Correspondingly, the concentration of produced CO increased from 1400 ppm to 13 000 ppm (Fig. 2; shown in orange). Furthermore, the Faradaic efficiency for CO formation (FE_{CO}) was highest at an applied current density of approximately 30 mA cm^{-2} (82%) but decreased sharply at both higher and lower current densities (ESI Fig. S4† shown in orange). The formation of H_2 accounted for the balance of gaseous products when FE_{CO} was <100%.

The surface morphology of the Ag catalyst surface before and after *i*-CO_2 reduction was monitored using a scanning electron microscope (ESI Fig. S5†). The lack of major morphological changes demonstrated the robustness of the catalytic material.

Simulation of thermoelectric reactive carbon electrolysis near geothermal plants

We next sought to integrate the TEG with our reactive carbon electrolyzer (Fig. 1). A standard reactive carbon electrolyzer requires a thermodynamic voltage of approximately 2.1 V to drive the *i*-CO_2 reduction reaction at the cathode, OER at the anode, and water splitting at the BPM.[32] We found that three commercially available thermoelectric generators (ESI Fig. S2†) connected in series (TEG) can produce voltages exceeding 2.1 V with a temperature difference (ΔT) of only 45 °C (Fig. 3). Furthermore, higher voltages and current densities can be achieved at higher ΔT values. To integrate the TEG into our reactive carbon electrolyzer, the positive terminal was connected to the anode, and the negative terminal to the cathode (ESI Fig. S3†). Voltage and current were measured in real-time using a voltmeter and an ammeter, respectively.

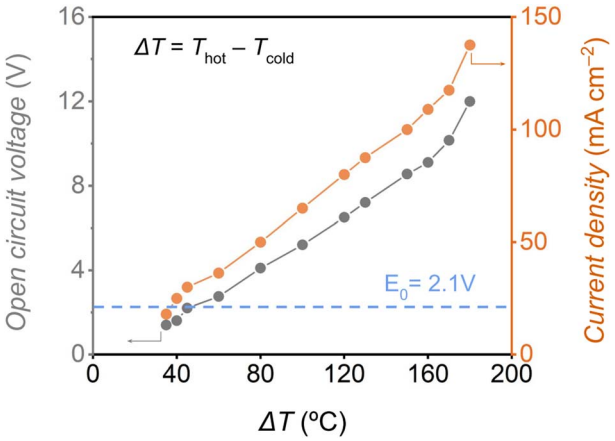

Fig. 3 Performance of three thermoelectric generators connected in series (TEG). The open circuit voltage and output current from TEG are plotted as a function of ΔT, where ΔT is the difference in temperature of the hot and cold plates of the TEG. The estimated Seebeck coefficient for the TEGs used in this study was measured to be 0.067 V K^{-1} (indicated by the slope of the gray line). A ΔT of 45 °C is required for the TEG to reach the minimum thermodynamic voltage of 2.1 V required to power a bicarbonate electrolyzer that converts *i*-CO_2 into CO (indicated by the blue dashed line).

To represent the typical temperatures observed at geothermal plants,[33] we varied T_{hot} from 80–200 °C, while T_{cold} was varied from 0–25 °C. The values of T_{hot} and T_{cold} were controlled and recorded in a similar manner as performed in a previous study where thermoelectric gas-fed electrolysis was performed.[27] As a result, a large range of ΔT ($T_{hot} - T_{cold}$) values were investigated (80–180 °C). Once ΔT reached a steady state (*i.e.*, temperature remained constant within ±1 °C), thermoelectrically-driven electrolysis of the reactive carbon solution was performed for 10 minutes, followed by the measurement of gaseous product concentrations by gas chromatography. To avoid affecting the performance of the electrolyzer by introducing heat into the system, we positioned the hot plate at least 15 cm away from it.

When operating our reactive carbon electrolyzer by thermoelectric power, we found that as ΔT was increased from 80 °C to 180 °C, the cell voltage increased from 2.3 V to 3.3 V, and the current density increased from 12 mA cm^{-2} to 70 mA cm^{-2} (Fig. 4a). The higher cell voltage at higher ΔT values follows the Seebeck equation, represented by eqn (1).[12] As a result, the concentration of *i*-CO_2 in the cathode chamber increased from 10 000 ppm to 30 000 ppm with a corresponding increase of CO from 2000 ppm to 15 000 ppm (Fig. 4b). The higher yield at higher ΔT values is a result of the increase in current density. These observations are indicative that the voltage generated from the TEGs can drive water dissociation at the BPM, generating protons that can react with HCO_3^- to form *i*-CO_2, according to eqn (4).

To gain an understanding of the efficiency of our thermoelectrically powered reactive carbon electrolyzer, we determined values for the Faradaic efficiency of CO formation (FE_{CO}) and CO_2 utilization efficiency (eqn (7)):

$$CO_2 \text{ utilization efficiency}(\%) = \frac{[CO]}{[CO_2] + [CO]} \times 100, \quad (7)$$

where [CO] is the concentration of CO produced during electrolysis and [CO_2] is the concentration of unreacted CO_2 from the reactor as measured by gas chromatography. We found that the CO_2 utilization efficiency increased from 12% at $\Delta T = 82$ °C to 63% at $\Delta T = 155$ °C (Fig. 4c). However, further increasing ΔT to approximately 180 °C decreases the CO_2 utilization efficiency to approximately 50%, likely due to mass transport limitations that can occur with increasing current.[34] Similarly, we determined that the FE_{CO} was greater than 50% across a ΔT range of 80–110 °C, with a maximum FE_{CO} of 82% at a ΔT of 110 °C (Fig. 4d). Further increases in ΔT above this range result in significant decreases in FE_{CO}. We show that the electrolyzer is durable over 12 hours, as determined by the stable measurements of cell voltage and CO concentration (Fig. 4e).

We then compared the results of our reactive carbon electrolyzer when powered by a potentiostat *versus* thermoelectrically (ESI Fig. S6†). Across a current density range of 15–70 mA cm^{-2}, the cell voltages for both cases were within experimental uncertainties. Furthermore, these current densities approximately doubled by using two sets of TEGs connected in parallel.[7]

Scaling up a thermoelectrically powered reactive carbon electrolyzer

We built a proof-of-concept system that connects a TEG to a reactive carbon electrolyzer with an active surface area of 100 cm^2 (10 cm × 10 cm; Fig. 5a, b and S7a ESI†). The cathode was prepared by automated spray coating of Ag nanoparticles on a 10 cm × 10 cm carbon paper (Fig. 5c). All other experimental parameters were identical to those used in our smaller scale (4 cm^2) system described above.

In terms of performance, we found that the cell voltage, current density and *i*-CO_2 and CO concentrations in the 100 cm^2 electrolyzer, all increased with an increase in ΔT (Fig. 5d and e), similar to what was observed for the 4 cm^2 electrolyzer. However, due to the larger surface area of the electrolyzer, the current density was reduced to 1–5 mA cm^{-2} (Fig. 5d; shown in orange) which is almost a factor of 20–25 times smaller than what was used for the 4 cm^2 electrolyzer. This decrease in the current density resulted in lower concentrations of CO (~100 times smaller than the 4 cm^2 electrolyzer) generated at the cathode (Fig. 5e; shown in orange). As a result, the total *i*-CO_2 concentration was affected by this smaller current density range observed in the 100 cm^2 electrolyzer (ESI Fig. S7b†). The current density-normalized *i*-CO_2 concentration increased from 429 ppm mA^{-1} cm^{-2} to 4000 ppm mA^{-1} cm^{-2} when the electrolyzer was scaled from 4 cm^2 to 100 cm^2. This is likely due to the voltage applied, which was beyond the potential needed to drive water dissociation at BPM to provide sufficient protons. These protons must react with HCO_3^- ions to generate *i*-CO_2, according to eqn (4). We also determined that the concentration of CO nearly doubles when two TEGs are connected in parallel (Fig. 5f) due to the current density doubling in this

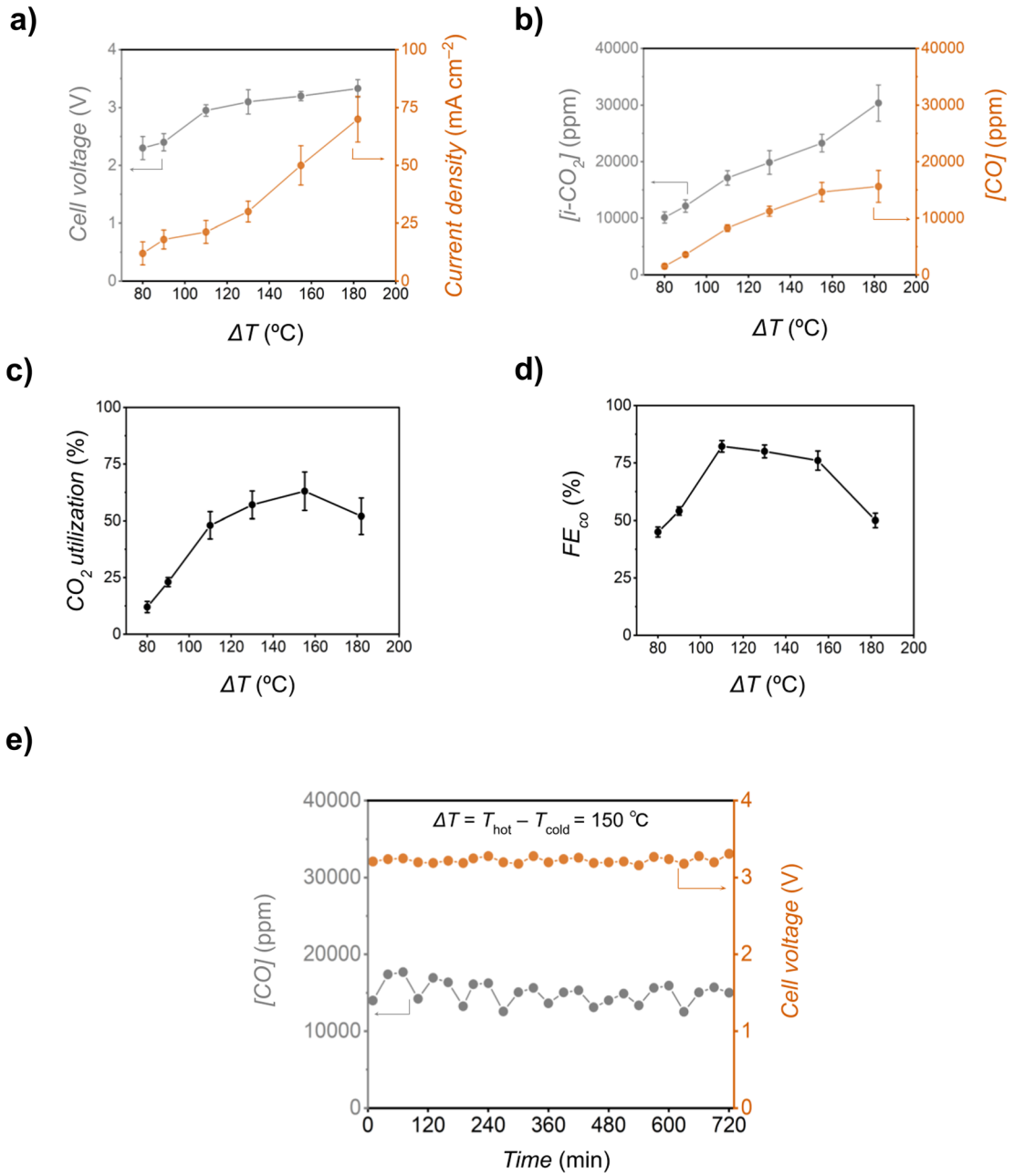

Fig. 4 Reactive carbon electrolysis driven by a TEG. (a) The dependence of cell voltage and current density with respect to the temperature difference employed (ΔT, which is equal to $T_{hot} - T_{cold}$). The T_{hot} was controlled by placing one face of the TEG in contact with a hotplate, and the T_{cold} was controlled with an ice-water bath placed in contact with the opposite face of the TEG. (b) The concentration of the *i*-CO_2 and CO (denoted as [*i*-CO_2] and [CO]) exiting from the cathode compartment as a function of ΔT. (c) CO_2 utilization values with respect to ΔT. (d) FE_{CO} values with ΔT. (e) A 12-hour stability experiment showing the variation [CO] and cell voltage ΔT of 150 °C with time (where T_{hot} was 165 °C and T_{cold} was 15 °C). The reactive carbon solution was replaced every 90 min, to maintain a stable pH of 8.2. The error bars represent the standard error from $n = 3$ independent experiments.

configuration.[27] We postulate that it may be possible to further increase the product concentration by connecting more TEGs in parallel.

Simulating thermoelectric reactive carbon electrolysis on Mars

The positive results we observed with our TEG-powered reactive carbon electrolyzer on a small (4 cm^2) and large (100 cm^2) scale prompted us to explore other potential applications for this technology. One such scenario is supporting human settlement on Mars. The Martian atmosphere consists primarily of CO_2 (>95%), and diurnal temperatures vary widely, ranging from −20 to −120 °C.[35] A biodome on Mars inhabited by humans could provide a T_{hot} of 25–30 °C, resulting in a ΔT range of 40–140 °C for thermoelectric generator operation. Another possible scenario is performing reactive carbon electrolysis during travel

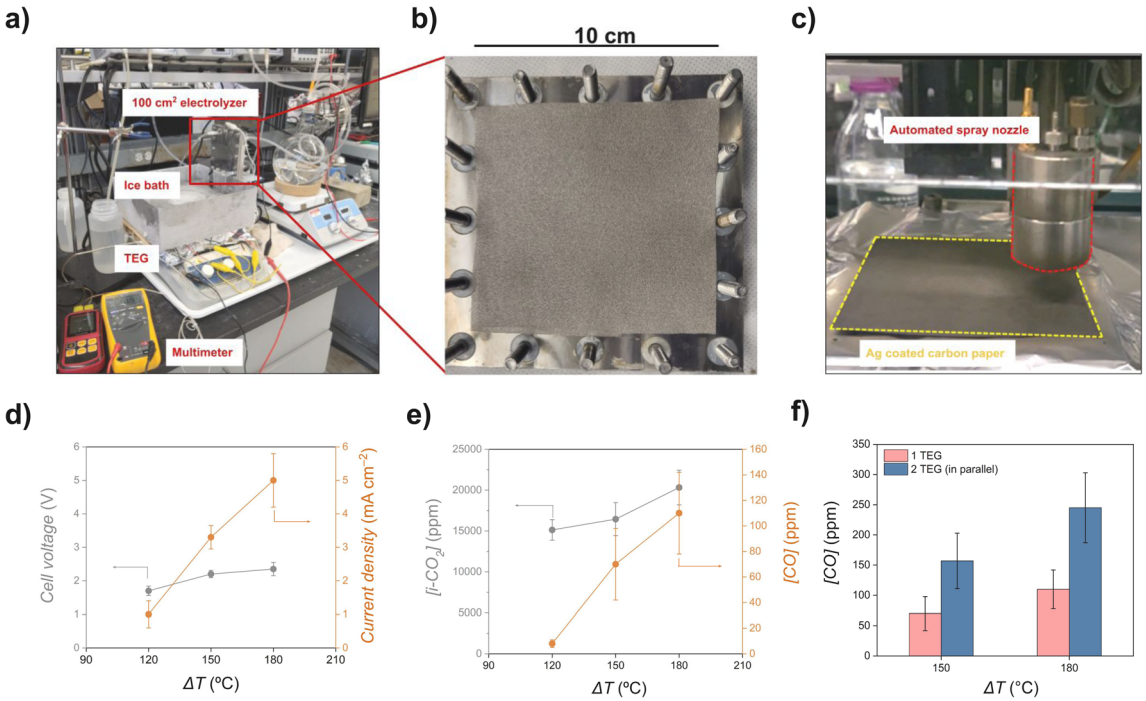

Fig. 5 Reactive carbon electrolysis driven by a TEG on a 100 cm^2 electrolyzer. (a) Experimental setup for thermoelectric driven electrolysis for a 10 cm × 10 cm electrolyzer. (b) The top view of the exposed area of the anode plate of the reactive carbon electrolyzer, showing the Ni foam. (c) An automated spray coater prepares a silver GDE on a 10 cm × 10 cm carbon paper. (d) The variation of cell voltage and current density with the temperature difference employed (ΔT which is equal to $T_{hot} - T_{cold}$). The T_{hot} was controlled by placing one face of the TEG in contact with a hotplate, and the T_{cold} was controlled with an ice-water bath placed in contact with the opposite face of the TEG. (e) The variation of the concentration of *i*-CO_2 and CO with respect to ΔT. (f) The improvement in CO performance metric at two ΔT values when two TEGs are connected in parallel. At ΔT of 150 °C, T_{hot} was 165 °C and T_{cold} was 15 °C. For ΔT of 180 °C, T_{hot} was 200 °C and T_{cold} was 25 °C. The error bars represent the standard error from $n = 3$ independent experiments.

to Mars. Thermoelectric generators could be installed on the spacecraft, using lightweight radiation sources (commonly employed by NASA)[36] to generate temperatures up to 200 °C, with ΔT values reaching 250–300 °C.

To test the first scenario, representing human settlement on Mars, we conducted reactive carbon electrolysis with a 4 cm^2 electrolyzer under conditions that simulate the Martian environment. A T_{cold} of approximately −75 °C (average diurnal temperature on Mars) was achieved by placing the cold face of the TEG in contact with an aluminum chamber containing a cryogenic ice bath made of dry ice and ethanol. T_{hot} was maintained at 25 °C by placing the TEG on a hotplate, while the electrolyzer itself was held at room temperature (20 °C). At a ΔT of 100 °C, the concentration of CO generated was approximately 535 ± 156 ppm (Fig. 6).

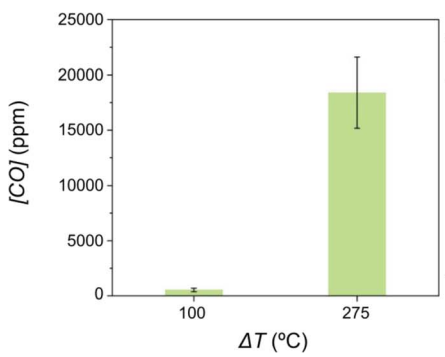

ΔT (°C)	T_{hot} (°C)	T_{cold} (°C)
100 (Scenario 1)	25	−75
275 (Scenario 2)	200	

Fig. 6 Simulation of thermoelectrically powered reactive carbon electrolyzer on Mars. The plot shows the variation of [CO] at two ΔT values. The T_{hot} was controlled by placing one face of the TEG in contact with a hotplate, and the T_{cold} was controlled with a dry ice-ethanol bath placed in contact with the opposite face of the TEG. The [CO] was recorded after ΔT reached a steady state and thermoelectric-driven electrolysis was ran for 10 minutes. The table presents two possible scenarios to achieve those two ΔT values. Scenario 1 represents human settlement on Mars and Scenario 2 represents travel to Mars. The error bars represent the standard error from $n = 3$ independent experiments.

To test the second possible scenario—reactive carbon electrolysis during travel to Mars—we conducted an experiment under high-temperature differentials, reaching a ΔT of up to 275 °C, which could be reasonably expected during the journey. In this setup, the hotplate temperature was set to 200 °C (achieved from lightweight radiation sources),[36] while the cold plate temperature was kept at −75 °C (Martian average). We observed that the CO concentration increased by a factor of 34 compared to the lower ΔT of 100 °C (Fig. 6). This increase was likely due to the higher current density (∼100 mA cm^{-2}), which is comparable to commercially available electrolyzer systems.

While using a gaseous CO_2 feedstock on Mars offers distinct advantages, trace amounts of O_2 (∼0.2%) and other impurities are present in the Martian atmosphere.[37] A reactive carbon electrolyzer is more resistant to impurities,[30,31] making it a more suitable solution for the electrochemical production of valuable chemicals on Mars.

Conclusions & recommendations

The integration of thermoelectric technology with reactive carbon electrolysis represents a new approach with several key advantages. First, it enhances CO_2 utilization efficiency by harnessing low-grade heat sources to offset energy demands. Second, this method supports global efforts to tap into renewable energy, providing a decentralized and robust energy solution that can be deployed in diverse settings, from industrial environments to remote locations with abundant geothermal resources. This study aimed to advance the landscape of carbon capture and utilization technologies by combining thermoelectric and electrochemical innovations, addressing the twin challenges of energy sustainability and carbon emission reduction.

Data availability

The data supporting the findings of the study are available within the paper and its ESI.†

Author contributions

A. S. and C. P. B. conceived the idea and interpreted the data. A. S. and S. M. performed the experiments and collected data. A. S. and S. M. wrote the first draft of the manuscript, G. V. C. advised and improved the manuscript. All authors participated in the discussion and final manuscript. C. P. B. supervised this project.

Conflicts of interest

The reactive carbon electrolyzer has been patented (*e.g.*, US Patent no. US12006580) and licensed, and C. P. B. is a founder of a company commercializing the technology. The remaining authors declare no other competing interests.

Acknowledgements

The authors are grateful to the Natural Sciences and Engineering Research Council of Canada (RGPIN-2024-06486), Canada Foundation for Innovation (229288), Canadian Institute for Advanced Research (BSE-BERL-162173), National Research Council of Canada's Materials for Clean Fuels Challenge program (MCF-128), and Canada Research Chairs for financial support.

References

1 D. M. Weekes, D. A. Salvatore, A. Reyes, A. Huang and C. P. Berlinguette, *Acc. Chem. Res.*, 2018, **51**, 910–918.
2 C. P. O'Brien, R. K. Miao, A. Shayesteh Zeraati, G. Lee, E. H. Sargent and D. Sinton, *Chem. Rev.*, 2024, **124**, 3648–3693.
3 W. A. Smith, T. Burdyny, D. A. Vermaas and H. Geerlings, *Joule*, 2019, **3**, 1822–1834.
4 B. Kanjilal, M. Nabavinia, A. Masoumi, M. Savelski and I. Noshadi, in *Advances in Carbon Capture*, ed. M. R. Rahimpour, M. Farsi and M. A. Makarem, Woodhead Publishing, 2020, pp. 29–48.
5 I. Sullivan, A. Goryachev, I. A. Digdaya, X. Li, H. A. Atwater, D. A. Vermaas and C. Xiang, *Nat. Catal.*, 2021, **4**, 952–958.
6 D. W. Keith, G. Holmes, D. St. Angelo and K. Heidel, *Joule*, 2018, **2**, 1635.
7 A. Soni, S. Ma, K. Ocean, K. Dettelbach, D. Lin, C. Rupnow, M. Mokhtari, C. Waizenegger, G. Crescenzo and C. Berlinguette, *ChemRxiv*, 2024.
8 Y. Hori, K. Kikuchi and S. Suzuki, *Chem. Lett.*, 1985, **14**, 1695–1698.
9 D. A. Salvatore, D. M. Weekes, J. He, K. E. Dettelbach, Y. C. Li, T. E. Mallouk and C. P. Berlinguette, *ACS Energy Lett.*, 2018, **3**, 149–154.
10 S. Overa, B. H. Ko, Y. Zhao and F. Jiao, *Acc. Chem. Res.*, 2022, **55**, 638–648.
11 D. J. D. Pimlott, Y. Kim and C. P. Berlinguette, *Acc. Chem. Res.*, 2024, **57**, 1007–1018.
12 B. A. Rosen, A. Salehi-Khojin, M. R. Thorson, W. Zhu, D. T. Whipple, P. J. A. Kenis and R. I. Masel, *Science*, 2011, **334**, 643–644.
13 S. Nitopi, E. Bertheussen, S. B. Scott, X. Liu, A. K. Engstfeld, S. Horch, B. Seger, I. E. L. Stephens, K. Chan, C. Hahn, J. K. Nørskov, T. F. Jaramillo and I. Chorkendorff, *Chem. Rev.*, 2019, **119**, 7610–7672.
14 X. Lu, C. Zhou, R. S. Delima, E. W. Lees, A. Soni, D. J. Dvorak, S. Ren, T. Ji, A. Bahi, F. Ko and C. P. Berlinguette, *Nat. Chem.*, 2024, **16**, 979–987.
15 D. R. Kauffman, J. Thakkar, R. Siva, C. Matranga, P. R. Ohodnicki, C. Zeng and R. Jin, *ACS Appl. Mater. Interfaces*, 2015, **7**, 15626–15632.
16 N. Zulkepli, J. Yunas, M. A. Mohamed and A. A. Hamzah, *Micromachines*, 2021, **12**, 734.
17 N. Jaziri, A. Boughamoura, J. Müller, B. Mezghani, F. Tounsi and M. Ismail, *Energy Reports*, 2020, **6**, 264–287.

18 C. S. R. Matthes, D. F. Woerner, T. J. Hendricks, J.-P. Fleurial, K. I. Oxnevad, C. D. Barklay and J. F. Zakrajsek, in *2018 IEEE Aerospace Conference*, 2018, pp. 1–9.
19 R. C. O'Brien, R. M. Ambrosi, N. P. Bannister, S. D. Howe and H. V. Atkinson, *J. Nucl. Mater.*, 2008, **377**, 506–521.
20 M. Hasebe, Y. Kamikawa and S. Meiarashi, in *2006 25th International Conference on Thermoelectrics*, 2006, pp. 697–700.
21 Y. Wang, Y. Zhang, X. Xin, J. Yang, M. Wang, R. Wang, P. Guo, W. Huang, A. J. Sobrido, B. Wei and X. Li, *Science*, 2023, **381**, 291–296.
22 A. P. Raman, W. Li and S. Fan, *Joule*, 2019, **3**, 2679–2686.
23 J. G. Morse, *Science*, 1963, **139**, 1175–1180.
24 P. Alegria, L. Catalan, M. Araiz, A. Rodriguez and D. Astrain, *Appl. Therm. Eng.*, 2022, **200**, 117619.
25 R. Y. Nuwayhid, D. M. Rowe and G. Min, *Renewable Energy*, 2003, **28**, 205–222.
26 S. Choo, F. Ejaz, H. Ju, F. Kim, J. Lee, S. E. Yang, G. Kim, H. Kim, S. Jo, S. Baek, S. Cho, K. Kim, J.-Y. Kim, S. Ahn, H. G. Chae, B. Kwon and J. S. Son, *Nat. Commun.*, 2021, **12**, 3550.
27 A. Soni, X. Lu, C. Zhou, S. Singh and C. P. Berlinguette, *Device*, 2024, **2**, 100603.
28 C. M. Jensen and D. W. Lee, *J. Chem. Educ.*, 2000, **77**, 629.
29 Z. Zhang, D. Xi, Z. Ren and J. Li, *Cell Rep. Phys. Sci.*, 2023, **4**, 101662.
30 D. J. D. Pimlott, A. Jewlal, B. A. W. Mowbray and C. P. Berlinguette, *ACS Energy Lett.*, 2023, **8**, 1779–1784.
31 D. J. D. Pimlott, A. Jewlal, Y. Kim and C. P. Berlinguette, *J. Am. Chem. Soc.*, 2023, **145**, 25933–25937.
32 T. Li, E. W. Lees, M. Goldman, D. A. Salvatore, D. M. Weekes and C. P. Berlinguette, *Joule*, 2019, **3**, 1487–1497.
33 J. N. Moore and S. F. Simmons, *Science*, 2013, **340**, 933–934.
34 S. Lu, Y. Wang, H. Xiang, H. Lei, B. B. Xu, L. Xing, E. H. Yu and T. X. Liu, *Journal of Energy Storage*, 2022, **52**, 104764.
35 *Welcome to the Planetary Data System*, **https://pds.nasa.gov/**, accessed 3 November 2024.
36 H. R. Williams, R. M. Ambrosi, N. P. Bannister, P. Samara-Ratna and J. Sykes, *Int. J. Energy Res.*, 2012, **36**, 1192–1200.
37 *Mars Education*, **https://marsed.asu.edu/mep/atmosphere**, accessed 13 October 2024.